Electronic Structure and Stability of Double Six-Membered Rings of Oxygen-Bridged Silicon and Aluminum Atoms Related to Cation Site Occupancy in FAU Zeolites: a DFT Study

Ellie L. Uzunova*,† and Hans Mikosch*,‡

Institute of General and Inorganic Chemistry, Bulgarian Academy of Sciences, Sofia 1113, Bulgaria, and Institute of Chemical Technologies and Analytics, Vienna University of Technology, Vienna 1060, Austria

Received: September 24, 2003; In Final Form: March 16, 2004

The electronic structure and relative stability of clusters with general composition $(M^{n+})_{x/n}H_{12}Si_{12-x}Al_xO_{18}$ with $x = 0, 2, 4$, $M = H^+$, Li^+, Na^+, K^+, Ca^{2+} forming double-six-membered rings (D_6R), are studied by the B3LYP method. In $Ca_2H_{12}Si_8Al_4O_{18}$ clusters, maximum separation of the Al atoms is favored, which implies a minimum number of Al−O−Si−O−Al linkages. A large number of isomers with Si,Al distributions strongly related to the type and location of the charge-compensating cations were determined for the ratio Si/Al = 5. All cations favor maximum separation of Al atoms within the T_6O_6 rings. Concurrent occupation of extraframework cation sites in the center of the D_6R and above the T_6O_6 window is energetically unfavorable for Li^+ and Na^+ cations, whereas this is achieved with K^+, in agreement with experimental data. The Si,Al ordering with one Al atom per T_6O_6 ring and at the largest distance within the D_6R is the most stable one with Li^+ and K^+ as extraframework cations, whereas Na^+ and Ca^{2+} favor the configuration with two Al atoms in one T_6O_6 ring. The small and medium size cations Li^+, Na^+, and Ca^{2+} approach the regions of high electron density in the D_6R. The HOMOs of both the siliceous fragments and the aluminum-containing fragments with the extraframework cations located near the four-membered ring walls consist mainly of O 2p nonbonding AOs. When the extraframework cations take up positions at the D_6R center, or near the T_6O_6 rings, the HOMOs O 2p nonbonding character is reduced: Al 3s and Al 3p AOs are admixed to the O 2p AOs. The maximum electron density is concentrated at the Al atoms and the Al-bonded oxygen atoms. When the Al atoms are in one T_6O_6 ring of a D_6R, the oxygen atoms of this ring bear a higher electron density. Lewis basic sites appear in proximity to the Brønsted acid sites in proton balanced clusters.

Introduction

Zeolites are aluminosilicates with a very open structure, formed by corner-sharing TO_4 tetrahedra, where T = Si and Al. The orientation of adjacent tetrahedra is not fixed, and the flexibility of the T−O−T angle permits the formation of cage-like polyhedra.[1,2] Extraframework cations compensate the negative framework charges, which arise from the substitution of tetrahedral Si atoms with lower-valence elements. These cations are positioned in the voids; they are loosely bound to the framework and are easily exchangeable. Two rules govern the Si,Al distribution in zeolites: Löwenstein's rule[3] for avoidance of Al−O−Al linkages and Dempsey's rule,[4] requiring maximum separation of the Al atoms (Si is favored at T-sites in the sequence T−O−Si−O−Al).

The unit cell of most zeolites consists of a large number of atoms (over 500), and it is convenient to segment it into smaller structural fragments: rings, prisms, and cages. In this approach, it is generally assumed that the overall framework stability is related to the relative stability of the individual building blocks. The cage- and prism-shaped silsesquioxanes $(HSiO_{3/2})_{2n}$, where $n = 2, 3$, etc., have been subjected to both experimental[5−7] and theoretical studies.[8−13] Structural fragments with three-membered rings experience considerable strain and proved to be of lower stability than the larger rings; in fact, they are not common for zeolites.[10a,13] Cages, consisting of 12 and 14 tetrahedral Si atoms and with a particular arrangement of the four- and five-membered rings, are known to be of the highest stability.[13] The D_6R unit is a secondary building unit (SBU) in a large number of zeolite structures: CHA, ERI, FAU, EMT, GME, LEV, OFF, EAB, KFI, LTL, LTN, and also in structural intermediates EMT/FAU.[1,2] The FAU structure consists of sodalite cages (truncated cuboctahedra) linked by D_6R as shown in Figure 1. The crystallographic equivalence of all T-sites in FAU simplifies the interpretation of the ^{29}Si NMR spectra, and a number of

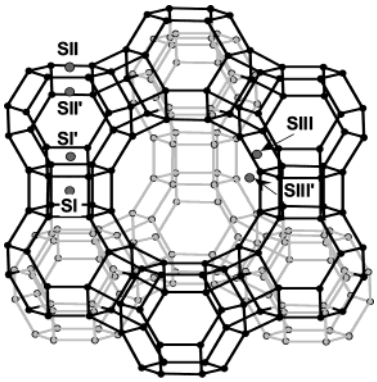

Figure 1. Schematic representation of the FAU zeolite framework with extraframework cation sites denoted. Oxygen atoms are not shown; they lie near the center of line segments, connecting T-atoms.

* To whom correspondence should be addressed.
† Bulgarian Academy of Sciences.
‡ Vienna University of Technology.

10.1021/jp036846h CCC: $27.50
Published on Web 05/01/2004

studies were devoted to the Si,Al distributions in these frameworks.[14−16] The cluster models, used for studying Si,Al ordering in FAU ranged from single-four- and six-membered rings (S_4R, S_6R), to two sodalite cages, connected by a D_6R.[15,17−19] The importance of D_6R as tertiary building unit in FAU crystallization was emphasized.[19] For most Si/Al ratios, it was found that more than one model ordering scheme was compatible with the Si,Al populations, derived from the NMR spectra. This uncertainty arises from the facts that a number of allowed Si,Al distributions can be fitted to maximum five NMR peaks and that the populations obtained from ^{29}Si NMR spectra are averaged over the whole sample, being unable to distinguish domains with different ordering. Comparison of experimental results with Monte Carlo simulations[20] leads to the conclusion that, at ratios higher than Si/Al = 4, deviations from Dempsey's rule were significant. For chabazite, another framework based on D_6R arranged in layers ABCABC and linked by tilted four-membered rings, specific Si,Al distributions were proposed. In the Si,Al ordering scheme, derived from NMR studies of samples with a ratio of Si/Al = 2.6, two Al atoms were placed at maximum distance within each T_6O_6 ring of two D_6R, whereas the third D_6R contained one Al per T_6O_6 ring.[21] A model based on symmetry considerations was proposed for CHA with composition $Ca_6Al_{12}Si_{24}O_{72}$, according to which Ca^{2+} ions are located on the surface of D_6R with 6Al atoms and in the center of D_6R with 3-fold symmetry, containing 3 Al atoms. Extended to FAU, this hypothesis states that a stable high-silica FAU should be built from D_6R with 3-fold symmetry, containing 6 or 3 Al atoms and entirely siliceous D_6R in violation of Dempsey's rule.[22] In chabazite, however, considerable changes in cation positions and framework geometry occur during ion exchange.[23] It has been recognized that extraframework cations play a major role in stabilizing particular Si,Al orderings, and recent Monte Carlo (MC), molecular dynamics (MD), and quantum-chemical (QC) studies have focused on the determination of the most favorable extraframework cation distributions.[24−26] In theoretical studies of the cation's properties, the importance of allowing free relaxation of the framework was outlined.[11,12]

The subject of the present study are $(M^{n+})_{x/n}H_{12}Si_{12-x}Al_xO_{18}$ clusters with $x = 0$, 2, and 4 in which SiO_4 and AlO_4 tetrahedra are connected via oxygen bridges; M = H^+, Li^+, Na^+, K^+, and Ca^{2+}. All of the Si,Al distributions are realistic for zeolite structures. The only restriction imposed comes from Löwenstein's rule for avoidance of Al−O−Al linkages. The maximum distance is maintained between extraframework cations in clusters with more than one cation. The electronic structure and relative stability of D_6R clusters with respect to Si,Al ordering and extraframework cation type and location are examined. Emphasis is placed on structural fragments with a ratio of Si/Al = 5, for which the extraframework cations are able to stabilize closely spaced Al atoms. The results obtained are expected to shed more light on cation-directed syntheses.

Methods

Geometry optimizations were performed in Cartesian coordinates by the B3LYP method, which includes local and nonlocal terms as implemented in the Gaussian 98 package.[27−30] The extraframework cations were positioned as found in FAU zeolites, see Figure 1.[31−35] The site SI lies in the center of the D_6R, SI′ on the opposite side of T_6O_6 faces of a D_6R and pointing to a sodalite cage, site SII at the center of a S_6R or displaced from this point into the supercage, site SII′ displaced from the center of a S_6R into the sodalite cage, site SIII in the supercage on a 2-fold axis opposite a S_4R between two 12-membered rings, and SIII′ near the four-ring edges and located in the 12-membered ring of the supercage. Cation sites near the D_6R of CHA are identical, with the exception that the extraframework position above the D_6R points into the CHA supercage. S_6R with the ratio of Si/Al = 3 were used to examine the Si,Al distribution, balanced by cations at the SII site; in the case of monovalent cations, the clusters were negatively charged. The D_6R clusters with Si,Al substitution were neutral, compensated by an appropriate number of positive charges. The standard 6-31G(d) basis set was employed for all atoms involved, with the exception of Ca^{2+} and K^+ for which the basis was extended to 6-311G(d). Hydrogen atoms were used to terminate the clusters via Si−H and Al−H bonds. For the OH-containing fragments, polarization functions at the hydrogen atoms were included via the 6-31G(d,p) basis. Harmonic frequency calculations were performed with all geometry optimized clusters, except two D_6R with lower symmetry (C_2 and C_s) and a Si/Al = 2 ratio, $Ca_2H_{12}Si_8Al_4O_{18}$. The points that correspond to minima (global or local) on the potential energy surface were identified by the absence of negative eigenvalues in the diagonalized Hessian matrix, which give rise to imaginary vibrational modes. For Na^+ containing clusters with coordination numbers lower than four and for extraframework cations at the SIII′ sites, the imaginary frequencies found at $\leq$ 40 cm^{-1} due to extraframework cation displacements were neglected.

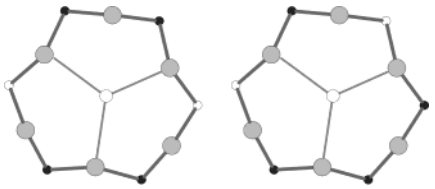

Figure 2. S_6R equilibrium geometry, as calculated by the DFT/B3LYP method. Atoms in decreasing size are O, M^+ (Li^+, Na^+, and K^+), and M^{2+} (Ca^{2+}), tetrahedral Si and Al. Oxygen atoms are large light gray circles, Si atoms are dark gray, Al atoms are small white circles, and extraframework cations are large white circles in the center. The sequence of T-atoms linking is denoted below each model.

Structure and Stability

S_6R with Si,Al Substitution. The S_6R are frequently used as cluster models for studying guest−host interactions in zeolite frameworks[36] and as a base for deriving force fields or potential functions.[37] They provide favorable oxygen coordination to cations and the SII site has the highest fractional occupancy in FAU zeolites.[32−35] The entirely siliceous rings with more than four tetrahedral atoms are very flexible and they exist in many conformations with rather close energies.[38] In studies of large-size transition metal cations occupying the SII site, certain coordinates were fixed during optimization.[36] The S_6R cluster models in the present study are with the ratio Si/Al = 3, and the two Al atoms are either placed at maximum distance within the S_6R or allow the formation of Al−O−Si−O−Al linkage as shown in Figure 2. Alkali and alkaline-earth cations have a high stabilization effect on the S_6R with Si,Al substitution; thus, no geometry restrictions were imposed. All cations favored maximum separation of the negative charges within the S_6R, in agreement with MD simulation studies and proving that for single-rings, Dempsey's rule is strictly obeyed.[50] Li^+ cations do not form a stable cluster with closely spaced Al atoms (Al−O−Si−O−Al linkages). The energy difference between clusters with Al−O−Si−O−Al linkages, when stabilized by Na^+, K^+,

TABLE 1: Relative Energies[a] (kJ mol^{-1}) of S_6R with Si/Al Substitution, Stabilized by Extraframework Cations at SII Sites as Calculated by B3LYP

cluster model/linkages	ΔE^0_{tot}	ΔE^{zpe}_{tot}	R_{M-O} (Å)[b]	R_{M-O} (Å)$_{exp.}$[34,35]
$[LiH_6Si_4Al_2O_6]^-$/Al−O−(Si−O)$_2$−Al	0.0	0.0	2.050; 3.492	
$[NaH_6Si_4Al_2O_6]^-$/Al−O−(Si−O)$_2$−Al	0.0	0.0	2.302; 3.221	
$[NaH_6Si_4Al_2O_6]^-$/Al−O−Si−O−Al	27.4	27.3	2.303; 3.141	2.36(3)
$[KH_6Si_4Al_2O_6]^-$/Al−O−(Si−O)$_2$−Al	0.0	0.0	2.701; 3.055	
$[KH_6Si_4Al_2O_6]^-$/Al−O−Si−O−Al	21.3	21.2	2.687; 2.921	2.663(7); 3.020(8)
$CaH_6Si_4Al_2O_6$/Al−O−(Si−O)$_2$−Al	0.0	0.0	2.402; 2.686	
$CaH_6Si_4Al_2O_6$/Al−O−Si−O−Al	21.7	21.5	2.399; 2.683	

[a] ΔE^0_{tot}, total energy difference (Hartree) relative to the lowest energy cluster $[M^IH_6Si_4Al_2O_6]^-$ or $M^{II}H_6Si_4Al_2O_6$; ΔE^{zpe}_{tot} includes zero-point corrections. $[LiH_6Si_4Al_2O_6]^-$: $E^0_{tot} = -2109.70369$; $[NaH_6Si_4Al_2O_6]^-$: $E^0_{tot} = -2264.45684$; $[KH_6Si_4Al_2O_6]^-$: $E^0_{tot} = -2702.07587$; $CaH_6Si_4Al_2O_6$: $E^0_{tot} = -2779.66848$. 1 Hartree = 2625.499748 kJ mol^{-1}. [b] M = Li^+, Na^+, K^+, and Ca^{2+} as extraframework charge compensating cations.

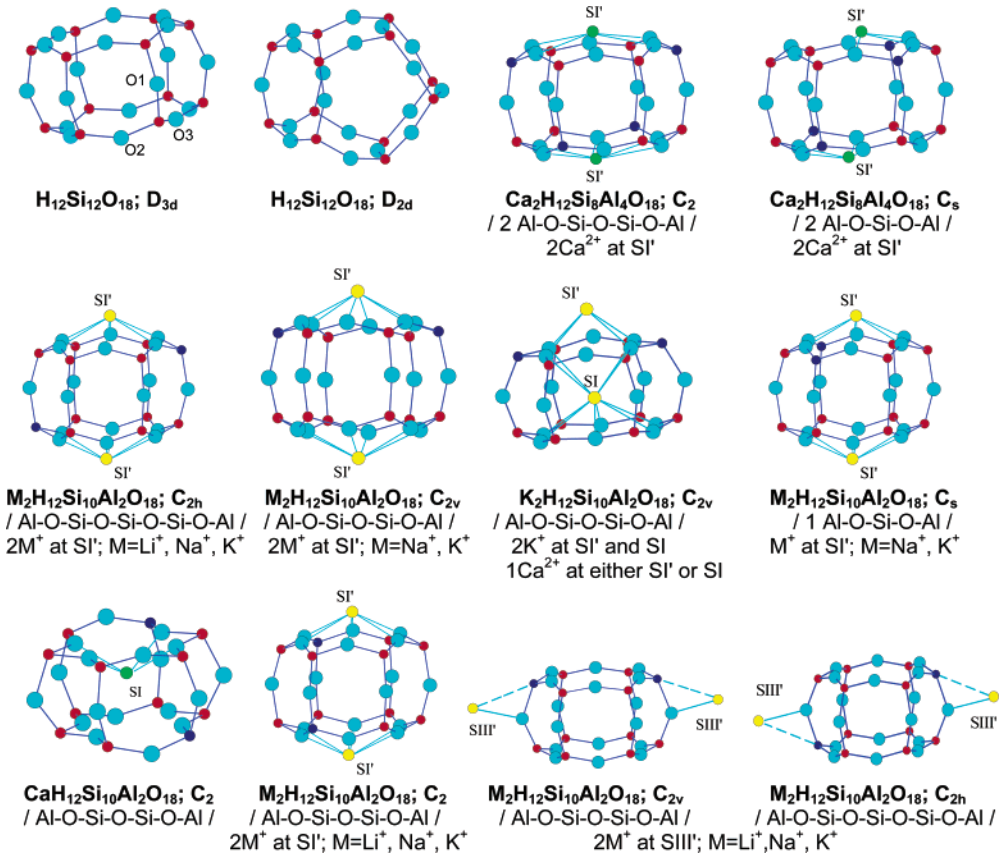

Figure 3. D_6R equilibrium geometry, as calculated by the DFT/B3LYP method. Atoms in decreasing size are O, M^+ (Li^+, Na^+, and K^+), and M^{2+} (Ca^{2+}), tetrahedral Si and Al. Oxygen atoms are light blue, M^{2+} atoms are green, M^+ atoms are yellow, Si atoms are red, and Al atoms are dark blue. The sequence of T-atoms linking and the extraframework cation positions are denoted below each model.

and Ca^{2+} as extraframework charge compensating cations, and the configurations with maximum negative charge separation (Al−O−(SiO)$_2$−Al linkages) is the largest for Na^+. The calculated M−O distances are very close to the experimental data, Table 1. The K^+ cations are significantly displaced from the plane of the six T-atoms; for the more stable configurations with Al−O−Si−O−Si−O−Al linkages, K^+ is located at 1.104 Å above the T_6 plane, whereas in the cluster containing one Al−O−Si−O−Al link, the displacement is even larger, 1.507 Å.

Cage-Shaped Silsesquioxanes. The optimization of $H_{12}Si_{12}O_{18}$ produced two stable isomeric structures with D_{3d} and D_{2d} symmetry, see Figure 3. The D_{3d} symmetry cluster is a D_6R with three discernible oxygen atom positions and it is a SBU in zeolite frameworks; it is iso-energetic with the D_{6h} symmetry fragment examined in previous studies by ab initio methods.[9b] The D_{2d} fragment is built of four- and five-membered rings (S_4R, S_5R) and it is cage-shaped. A synthetic material, based on the D_{2d} structure, has been synthesized, and the crystal structure data are in agreement with our B3LYP-calculated bond lengths and angles as shown in Table 2.[39] The D_{2d} structural fragment proved to be more stable relative to the D_6R with D_{3d} symmetry; both fragments have high HOMO−LUMO energy gaps, see Table 3. The small energy spacing between the two structural fragments indicates a smooth potential energy surface for the T_{12} polysiloxanes. Although S_5R is SBU in a large group of synthetic zeolites (the pentasils), structural fragments that are similar to the D_{2d} isomer are not common for zeolites. The D_6R fragment forms a structure of lower density and higher symmetry. Via the six-membered rings, it is able to connect larger cage-shaped polyhedra like the sodalite cages.

D_6R with Si,Al Substitution. In D_6R of D_{3d} symmetry, the cations centered above the T_6O_6 plane have three oxygen atoms as nearest neighbors and another three oxygen atoms as next nearest neighbors. Si,Al substitution lowers the symmetry of the D_6R, which undergoes also a slight deformation, because

TABLE 2: Average Bond Lengths and Angles for D_6R Fragments Calculated by B3LYP

cluster model/ cation site occupation	R_{Si-O} (Å)	R_{Al-O} (Å)	∠Al−O−Si (deg)	∠Si−O−Si (deg)	∠O−Al−O (deg)	∠O−Si−O (deg)	R_{M-O} (Å)[a]
D_{2d}; $H_{12}Si_{12}O_{18}$	1.637			154.0		109.7	
D_{2d}; $R_{12}Si_{12}O_{18(exp)}$[39]	1.61÷1.62			145÷158		108÷115	
D_{3d}; $H_{12}Si_{12}O_{18}$	1.639			150.3		109.7	
C_{2h}; $M_2H_{12}Si_{10}Al_2O_{18}$							
2 Li^+ at SI′	1.635	1.794	138.0	137.2	105.3	109.3	1.985; 2.124
2 Li^+ at SIII′	1.635	1.763	148.0	149.7	112.7	109.1	1.798
2 Na^+ at SI′	1.642	1.773	152.8	148.8	104.3	107.9	2.420; 3.166
2 Na^+ at SIII′	1.640	1.754	145.9	152.4	113.2	110.7	2.162
2 K^+ at SI′	1.634	1.779	150.9	153.5	109.8	108.8	2.691; 2.827; 3.086
2 K^+ at SIII′	1.642	1.762	145.6	152.4	112.3	110.3	2.499
C_{2v}; $M_2H_{12}Si_{10}Al_2O_{18}$							
2 Li^+ at SIII′	1.639	1.764	148.1	147.0	112.5	108.7	1.801
2 Na^+ at SI′	1.630	1.790	144.7	145.6	104.3	108.4	2.323; 2.353 3.137; 3.373
2 Na^+ at SIII′	1.639	1.755	144.8	152.8	112.9	110.4	2.166
$NaX_{(exp)}$[34]	1.631÷1.651	1.701÷1.714			109.6	109.8	2.267; 2.933
2 K^+ at SI′	1.628	1.788	150.2	149.4	108.8	108.2	2.709; 3.342
K^+ at SI and SI′	1.642	1.772	140.1	149.1	109.5	107.8	2.734; 2.867 3.032; 3.663
2 K^+ at SIII′	1.629	1.761	145.3	152.5	112.3	110.8	2.500
$KX_{(exp)}$[35]	1.667				107.7÷111.5		2.475÷3.335
Ca^{2+} at SI	1.647	1.810	132.8	138.3	100.1	108.3	2.392; 2.780
Ca^{2+} at SI′	1.640	1.789	141.7	148.4	103.8	108.4	2.289; 3.258
$CaY_{(exp)}$[40]	1.633÷1.671		129.0÷161.0		106.0÷112.0		
C_s; $M_2H_{12}Si_{10}Al_2O_{18}$							
2 Li^+ at SIII′ at AlOSi	1.636	1.766	147.9	150.6	111.7	109.0	1.798
2 Na^+ at SI′	1.650	1.793	145.9	150.8	108.6	111.2	2.299÷2.530 2.950; 3.511
2 K^+ at SI′	1.624	1.786	150.5	152.7	105.5	107.3	2.719÷2.790 2.921; 3.240
C_2; $M_2H_{12}Si_{10}Al_2O_{18}$							
2 Li^+ at SI′	1.634	1.776	140.1	142.4	102.4	109.5	1.890; 2.021
2 Na^+ at SI′	1.644	1.788	144.8	150.3	107.9	110.8	2.288; 2.430
2 K^+ at SI′	1.635	1.778	148.9	151.2	108.7	109.8	2.678; 2.721
Ca^{2+} at SI	1.644	1.784	135.6	140.1	102.2	107.9	2.330; 2.463
C_2; $Ca_2H_{12}Si_8Al_4O_{18}$; 2 Ca^{2+} at SI′	1.647	1.793	145.1	149.0	106.7	107.2	2.295; 2.311 3.270
C_s; $Ca_2H_{12}Si_8Al_4O_{18}$; 2 Ca^{2+} at SI′	1.638	1.784	147.7	154.8	103.1	107.3	2.293; 2.382 3.146

[a] M = Li^+, Na^+, K^+, and Ca^{2+} as extraframework charge compensating cations.

Al−O bonds are longer than the Si−O bonds. Depending on the type of the extraframework cation, the SI sites in the center of the D_6R and the SI′ sites, located above and below the T_6O_6 planes, respectively, may move toward the Al atoms, because the cations tend to approach the regions of high electron density. The calculated bond lengths (Si−O and Al−O) and valence angles (∠O−T−O, ∠T−O−T), presented in Table 2 are in agreement with experimental crystal structure data for FAU zeolites.[34,35,40,41] A general trend is that ∠OAlO is larger than ∠OSiO, when the extraframework cations occupy SIII′ sites. The ∠OAlO is smaller than ∠OSiO, when the SI′ sites are filled by small (Li^+) and medium size cations (Ca^{2+} and Na^+). The largest angle deformation is caused by Ca^{2+} at the central position SI inside the D_6R, defining the smallest values of ∠OAlO, ∠AlOSi and ∠SiOSi.

D_6R with Bridging Hydroxyl Groups, $H_{12}Si_{10}Al_2O_{16}(OH)_2$. The protons as charge-compensating cations form stable D_6R fragments with bridging hydroxyl groups Al−(OH)−Si. The four schemes of Si,Al ordering for the ratio of Si/Al = 5, examined in the present study are shown in Figure 4. Depending on the sites occupied by Al atoms, fragments with C_{2h}, C_{2v}, C_2, and C_s symmetry are obtained. The configuration with one Al atom per T_6O_6 ring at maximal distance within the D_6R yields clusters of C_{2h} symmetry. The C_{2v} symmetry clusters contain both Al atoms in one T_6O_6 ring at maximal distance within the ring. C_2 symmetry fragments are formed with two Al atoms in the opposite T_6O_6 rings, but each Al placed on a T-site of adjacent T_4O_4 rings at maximum distance. The difference from C_{2v} symmetry clusters is that the Al−O−(Si−O)$_2$−Al linkages are not part of the T_6O_6 ring; the Al−Al distance in the C_2 symmetry fragments should be at least 0.30 Å larger, than in the C_{2v} fragments, based on average T-site coordinates from structure determinations.[1b] Minor deformations of the D_6R due to the actual difference between Al−O and Si−O bond lengths increase the variation in Al−Al interatomic distance to 0.55−0.65 Å. The C_s symmetry fragments permit closely spaced Al atoms, separated by only one Si atom.

The OH groups are formed with the oxygen atoms O1, connecting the two T_6O_6 rings. The proton, attached to an O1 atom in FAU, points to the supercage and is of lowest energy, compared with O2, O3, and O4 sites.[43,45] The energy spacings between different Si,Al orderings are small, within 7−8 kJ mol^{-1}, see Table 3; the C_{2v} and C_s symmetry fragments are nearly isoenergetic. The calculated bond lengths and OH-stretching vibrational frequencies are in agreement with the available experimental data as shown in Table 4. They are not affected by the different Si,Al orderings.

D_6R with C_{2h} and C_{2v} Symmetry, $(M^n)_{2/n}H_{12}Si_{10}Al_2O_{18}$. Deviations from Dempsey's rule were established for FAU zeolites in the region of high Si/Al ratios and both the simulation and

TABLE 3: Relative Energies[a] (kJ mol^{-1}) of D_6R and HOMO−LUMO Energy Gaps (eV) Calculated by B3LYP

cluster model	ΔE^0_{tot}	ΔE^{zpe}_{tot}	HOMO−LUMO
D_{2d}; $H_{12}Si_{12}O_{18}$	0.0	0.0	9.10
D_{3d}; $H_{12}Si_{12}O_{18}$	12.9	13.5	9.14
$H_{12}Si_{10}Al_2O_{16}(OH)_2$			
C_2; Al−O−(Si−O)$_2$−Al	0.0	0.0	8.11
C_{2h}; Al−O−(Si−O)$_3$−Al	7.2	5.8	8.09
C_{2v}; Al−O−(Si−O)$_2$−Al	14.1	13.1	7.98
C_s; Al−O−Si−O−Al	15.5	15.2	7.84
$Li_2H_{12}Si_{10}Al_2O_{18}$			
C_{2h}; 2 Li^+ at SI′	0.0	0.0	8.01
C_2; 2 Li^+ at SI′	44.6	45.5	7.57
C_{2h}; 2 Li^+ at SIII′	277.5	274.3	6.28
C_{2v}; 2 Li^+ at SIII′	280.0	278.2	6.28
C_s; 2 Li^+ at SIII′	285.3	280.4	6.17
$Na_2H_{12}Si_{10}Al_2O_{18}$			
C_{2v}; 2 Na^+ at SI′	0.0	0.0	6.75
C_2; 2 Na^+ at SI′	15.5	13.9	6.95
C_{2h}; 2 Na^+ at SI′	32.6	28.8	6.86
C_s; 2 Na^+ at SI′	36.0	32.9	6.50
C_{2h}; 2 Na^+ at SIII′	247.6	244.3	5.47
C_{2v}; 2 Na^+ at SIII′	252.3	248.4	5.46
$K_2H_{12}Si_{10}Al_2O_{18}$			
C_{2h}; 2 K^+ at SI′	0.0	0.0	6.74
C_{2v}; 2 K^+ at SI′	8.4	8.6	6.34
C_2; 2 K^+ at SI′	13.0	13.1	6.61
C_s; 2 K^+ at SI′	28.5	27.6	6.06
C_{2v}; K^+ at SI and SI′	39.0	38.9	6.95
C_{2h}; 2 K^+ at SIII′	214.4	213.4	5.52
C_{2v}; 2 K^+ at SIII′	219.5	218.0	5.48
$CaH_{12}Si_{10}Al_2O_{18}$			
C_{2v}; Ca^{2+} at SI	0.0	0.0	8.12
C_{2v}; Ca^{2+} at SI′	7.0	6.6	6.27
C_2; Ca^{2+} at SI	19.8	21.0	8.06
$Ca_2H_{12}Si_8Al_4O_{18}$			
C_2; 2 Ca^{2+} at SI′	0.0	-	6.13
C_s; 2 Ca^{2+} at SI′	49.8	-	5.88

[a] ΔE^0_{tot}, total energy difference (Hartree) relative to the lowest energy cluster $(M^{n+})_{x/n}H_{12}Si_{12-x}Al_xO_{18}$; ΔE^{zpe}_{tot} includes zero-point corrections. D_{2d}, $H_{12}Si_{12}O_{18}$: $E^0_{tot} = -4836.98709$; C_2, $H_{12}Si_{10}Al_2O_{16}(OH)_2$: $E^0_{tot} = -4744.07419$; C_{2h}, $Li_2H_{12}Si_{10}Al_2O_{18}$: $E^0_{tot} = -4758.20315$; C_{2v}, $Na_2H_{12}Si_{10}Al_2O_{18}$: $E^0_{tot} = -5067.71441$; C_{2h}, $K_2H_{12}Si_{10}Al_2O_{18}$: $E^0_{tot} = -5942.96413$; C_{2v}, Ca^{2+} at SI, $CaH_{12}Si_{10}Al_2O_{18}$: $E^0_{tot} = -5420.65345$; C_2, $Ca_2H_{12}Si_8Al_4O_{18}$: $E^0_{tot} = -6004.36187$. 1 Hartree = 2625.499748 kJ mol^{-1}.

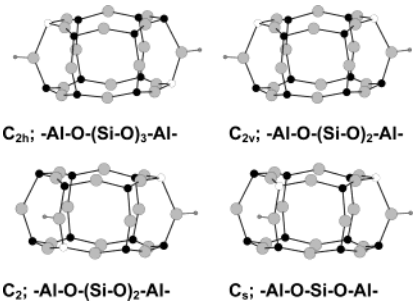

Figure 4. Formation of bridging hydroxyl groups Al−(O1H)−Si in proton-balanced clusters with a ratio of Si/Al = 5 and variable Si,Al ordering.

experimental studies of cation site occupancies diverged to a certain extent.[20,24−26,47] Na^+ cations were a subject of MC and MD simulation studies and the cation sites SIII′ have been correctly reproduced, though they are with low fractional occupancy. Li^+, K^+, and Ca^{2+} as extraframework cations have received less attention. Recent MD simulations of CaLSX (Si/Al = 1) found no cations at SI′ sites,[26] but according to X-ray and neutron diffraction studies, this site is at least 15% occupied.[41]

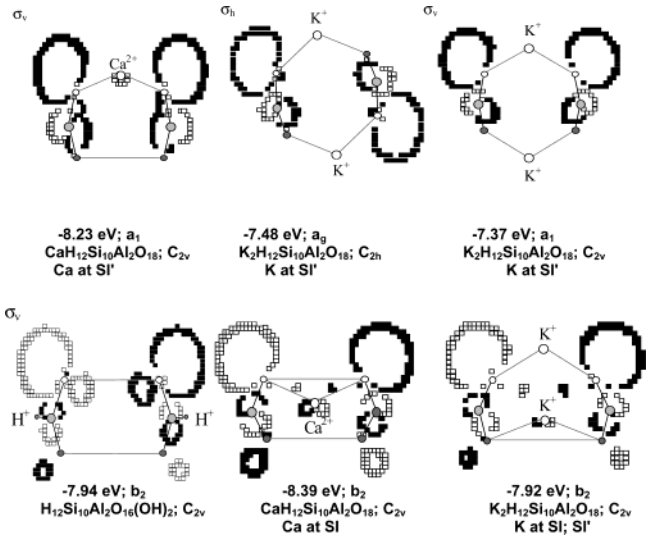

Figure 5. HOMO contour plots in the denoted symmetry planes. Atomic nuclei are represented by open circles, the oxygen atoms being light gray large circles, Si atoms are gray circles, and Al atoms are white circles. Extraframework cations, white large circles, and protons, small gray circles, are specifically denoted. The positive parts of the orbitals are depicted by filled squares and the negative part is depicted by open squares. Orbital contours correspond to 90% electron density.

The high-silica region in our study is represented by D_6R clusters of the Si/Al = 5 ratio. The C_{2h} symmetry fragments enclose one Al atom per T_6O_6 ring, /AlO(SiO)$_3$Al/ sequence, see Figure 3, and they are of highest stability with Li^+ or K^+ as charge-compensating cations at SI′ site, as shown in Table 3. It should be noted that Ca^{2+} does not form a stable D_6R of C_{2h} symmetry. A larger number of stable clusters emerge from the D_6R fragments with C_{2v} symmetry, /AlO(SiO)$_2$Al/ sequence. In the C_{2v} fragment, Ca^{2+} may occupy either the SI′ site above the $Si_4Al_2O_6$ ring or the SI site inside the D_6R, the central position for the cation being more favorable. K^+ cations can be found at SI and SI′ sites and a fragment with both sites occupied is about 30 kJ mol^{-1} higher in energy than the one with K^+ located at opposite sides of the T_6O_6 rings. The calculated internuclear distance (3.67 Å) between two K^+ at SI and SI′ sites of the same D_6R is slightly shorter than the experimental one (3.87 Å).[35b] This particular cation arrangement is achieved only with K^+, and the cation−cation distance is the shortest registered in FAU zeolites. The K^+ cation at SI site is in this case shifted from the center of the D_6R by 0.3 Å as a result of repulsion forces between cations. Li^+ and Na^+ do not reside in the center of a D_6R, when another cation is positioned at the SI′ site. This result agrees with the experimental observations that, although the fractional occupancy of the SI site in Y zeolites may reach 60%,[47] in X zeolites no Na^+ is found inside the D_6R.[33,34] According to MD studies, Na^+ cations in Y zeolites cannot attain optimal oxygen coordination in the center of the D_6R and are displaced by 0.6 Å in the direction of the T_6O_6 ring.[24] Na^+ and Ca^{2+} have very close ionic radii of 1.00 and 1.02 Å, respectively; the ionic radius of K^+ is larger, 1.38 Å.[48] All cations are small enough, compared with the free aperture of the T_6O_6 ring (5.29 Å).[49] The displacement of the SI′ site from the ring plane depends on the type of the extraframework cation. Na^+ and Ca^{2+} at SI′ sites create a higher positive electrostatic field than K^+, and they are located very close to the T_6O_6 plane. The strong repulsive forces prevent another cation from occupying the site at the center of the prism.

Instead of reaching maximum negative charge separation within the D_6R, both Na^+ and Ca^{2+} form more stable clusters

TABLE 4: Harmonic Stretching Vibrations and Selected Internuclear Distances of Bridging Hydroxyl Groups in Al−(OH)−Si

model	$R_{O(1)-H}$ (Å)	∠Al−O(1)H−Si deg	$R_{Al-HO(1)}$ (Å)	O(1)−H frequency cm^{-1}
$H_{12}Si_{10}Al_2O_{16}(OH)_2$				
C_2; Al−O−(Si−O)$_2$−Al	0.969	133.5	2.477	3821
C_{2h}; Al−O−(Si−O)$_3$−Al	0.968	134.4	2.488	3828
C_{2v}; Al−O−(Si−O)$_2$−Al	0.968	135.0	2.490	3826
C_s; Al−O−Si−O−Al	0.968	132.6	2.496	3824
DFT/SMP[a] (FAU)[42]	0.970	129.8	2.460	3723
DFT/LDA[b] (FAU)[43]	0.980	128.7	2.490	3731
experiment (FAU)[44−46]		135.7	2.48 ± 0.04	3787[c]

[a] Shell model potential. [b] Local density approximation. [c] Harmonic frequency, calculated from the experimentally observed anharmonic vibration.

with two Al atoms placed in one T_6O_6 unit and stabilize AlO(SiO)$_2$Al linkages relative to AlO(SiO)$_3$Al linkages, see Table 3. The latter can be explained by comparing the Na−O distances in these clusters. In the C_{2v} fragment, the two Na^+ are coordinated to four oxygen atoms each, at distances 2.32−2.35 Å and the remaining oxygen atoms are at distances 3.13 Å (in the Si_6O_6 ring) and 3.37 Å (in the $Si_4Al_2O_6$ ring). The Na−Al internuclear distance is 3.08 Å. In the C_{2h} fragment, each Na^+ cation is at a distance of 2.42 Å from the nearest four oxygen atoms and at 3.16 Å from the remaining two oxygen atoms in the Si_5AlO_6 ring; the Na−Al distance in this case is 3.20 Å. The energy difference between the two fragments should be attributed to a more favorable position of the Na^+ cations with respect to the centers, bearing the negative framework charge. The distance from the extraframework cations to the ring plane, defined by the six T atoms, increases with increasing their ionic radii. In C_{2v} fragments, Ca^{2+} is found at 0.88 Å above the $Si_4Al_2O_6$ ring, Na^+ is at 0.85 Å from the $Si_4Al_2O_6$ ring and at 1.05 Å from the Si_6O_6 ring. The SI sites inside the D_6R are energetically slightly more favorable for Ca^{2+}, see Table 3; the cation is in this case displaced from the D_6R center by 0.4 Å in the direction of the $Si_4Al_2O_6$ ring. When both SI′ sites are occupied by K^+ in either C_{2h} or C_{2v} clusters, the cation is found at approximately equal distance (1.55−1.60 Å) from the two Si_5AlO_6, the $Si_4Al_2O_6$, or the Si_6O_6 ring. Maximum separation of the negative framework charge within the D_6R is favored, but the energy differences between the C_{2h} and the C_{2v} fragments are smaller, compared to the values obtained with Na^+. The general trend is decreasing the interatomic distance between the charge-compensating cations and the nearest oxygen atoms in the order $K^+ > Na^+ > Ca^{2+} > Li^+ > H^+$. The energy variation between clusters with Si_5AlO_6 rings only and those, containing one $Si_4Al_2O_6$ and one Si_6O_6 ring, is very small, when the charge-compensating cations take up the SIII′ sites, particularly for Li^+. All clusters with cations at SIII′ sites are of much higher energy than others with SI, SI′ site occupation, see Table 3. The calculated NaIII′−O1 distances are shorter than the experimental data; however, the experimental values for different FAU samples diverge by 0.14 Å.[33,34] Compared with the other extraframework sites, the SIII′ sites are coordinatively unsaturated and a large fraction remains vacant in the zeolite framework.[33−35]

D_6R with C_2 and C_s Symmetry, $(M^n)_{2/n}H_{12}Si_{10}Al_2O_{18}$ and $(M^{II})_2H_{12}Si_8Al_4O_{18}$. The formation of Al−O−Si−O−Al linkages in one T_6O_6 ring of the clusters with a Si/Al = 5 ratio lowers further the symmetry to C_s, see Figure 3. Both Na^+ and K^+ at SI′ sites form such lower symmetry fragments. The increase in the relative energy is comparable to the creation of such linkages in D_4R.[12] The more polarizable cation K^+ can stabilize closely spaced Al atoms in T_6O_6 better than the Na^+ cation, see Table 3. Li^+ at SI′ sites form a stable cluster with C_2 symmetry, whereas neither a C_{2v} nor a C_s symmetry fragment could be stabilized, because the cations positioned at the Si_6O_6 ring could not reach a favorable coordination by oxygen atoms: the Li^+−O distance remained too long. In general, the clusters containing Al−O−Si−O−Al linkages (C_s symmetry) are less stable than the clusters with larger separation of the negative charges. With K^+ at SI′ sites, the energy difference between the C_{2v} and C_2 symmetry clusters was rather small. It is worthwhile noting that the C_2 symmetry fragments with Na^+ and K^+ cations at SI′ sites, as well as Ca^{2+} at the SI site in clusters with a ratio of Si/Al = 5, are less stable than those with C_{2v} symmetry, in which the two Al atoms are in one T_6O_6 ring and at shorter distance. Examination of the molecular orbital coefficients reveals that when the two Al atoms are in one T_6O_6 ring, the electron density is delocalized among the oxygen atoms of the same ring. In the clusters of C_2 symmetry, the negative charge is delocalized over O1, O2, and O3 atoms bonded to the Al atom, but O1 atoms do not provide favorable coordination to SI and SI′ extraframework sites. In the case of proton-balanced clusters, where the bridging hydroxyl groups are formed with O1 atoms as shown in Figure 4, the C_2 symmetry fragment is of highest stability, see Table 3.

Divalent charge-compensating cations Ca^{2+} positioned above the T_6O_6 ring planes (SI′ sites) were considered for clusters with a Si/Al = 2 ratio. In the C_2 symmetry cluster, maximum separation of the negative charges in the $Si_4Al_2O_6$ rings is preserved. Al−O−Si−O−Al linkages in each T_6O_6 ring are allowed to occur in the C_s symmetry fragment, as illustrated in Figure 3. It should be noted that Al−O−Si−O−Al linkages exist in both isomers, but their number increases by two in the C_s fragment. The maximum separation of negative charges within the T_6O_6 rings is definitely favored, see Table 4. Summarizing the results on S_6R and D_6R with Ca^{2+} as charge-balancing cations, we may conclude that Ca^{2+} allow the formation of Al−O−Si−O−Al linkages at ratios Si/Al < 3.

Molecular Orbitals

The HOMO of the two silsesquioxane cages with D_{2d} and D_{3d} symmetry is O 2p nonbonding AO. The HOMO−LUMO energy gap is very high for these clusters, see Table 4, and it is 1 eV higher as compared with tetragonal prisms.[12] At Al/Si > 0 ratios, when the negative framework charge is compensated by extraframework cations (Li^+, Na^+, K^+, Ca^{2+}, and H^+), the HOMO electron density is redistributed, depending on the cation's location. With Li^+, Na^+, and K^+ occupying the SIII′ sites, the HOMO retains fully its O 2p nonbonding character and it is delocalized over all oxygen atoms. The HOMO−LUMO energy gap is the lowest for these fragments. In proton-balanced D_6R, containing bridging hydroxyl groups Al−(OH)−Si, and in D_6R with cations, located at SI′ positions, the O 2p nonbonding character of the HOMO is reduced. Comparison of the MO coefficients reveals that the electron density is concentrated at the Al atom and the oxygen atoms that are bonded to Al. Thus, it retains some oxygen lone-pair character,

with Al 3s and Al 3p AOs admixed. With charge-balancing cations located at the center of the prism, site SI, the O 2p nonbonding character of the HOMO is further reduced; it consists of O 2p, Al 3s, Al 3p, Si 3s, and Si 3p AOs. Bringing together the negative framework charges in one T_6O_6 ring results in an increased HOMO electron density on the oxygen atoms of that ring, when extraframework cations occupy the SI or SI′ sites. In proton-balanced clusters with bridging hydroxyl groups Al−(O1H)−Si, the O2 and O3 atoms connected to Al atoms acquire the highest HOMO density and form Lewis basic sites.

The LUMO is extended over the extraframework cations and it is evenly distributed between the two positive charges, when they have equivalent locations. The same holds for K^+ at the nonequivalent positions SI and SI′ as in this case both cations are coordinatively saturated. For K^+ and Na^+ taking SI′ sites in C_{2v} fragments, the highest LUMO density is on the cation, facing the Si_6O_6 ring, whereas the next lowest unoccupied orbital is over the cation, positioned near the negative framework charges. According to these results, it is possible to discriminate quantitatively the reactivity of cations in Si_6O_6 environment and those near $Si_{6-x}Al_xO_6$ rings as nucleophilic centers.

Conclusions

DFT studies of D_6R structural fragments $(M^{n+})_{x/n}H_{12}Si_{12-x}Al_xO_{18}$ with $x = 0$, 2, and 4, in which the negative charge, arising from Si,Al substitution is compensated by Ca^{2+}, Li^+, Na^+, K^+, and H^+, reveal that different Si,Al orderings can be stabilized by the small (Li^+ and H^+) and medium size (Na^+ and Ca^{2+}) cations. At a ratio of Si/Al = 2, maximum separation of the negative charges is favored. At a ratio of Si/Al = 5, some particular Si,Al orderings become more stable when a favorable coordination of the extraframework charges by oxygen atoms from the T_6O_6 rings is reached. K^+ spans the highest number of stable isomers and occupation of SI and SI′ in one D_6R is allowed. The medium size cations (Na^+ and Ca^{2+}) stabilize the Al−O−(Si−O)$_2$−Al linkages with respect to Al−O−(Si−O)$_3$−Al linkages. For $Na_2H_{12}Si_{10}Al_2O_{18}$, this conclusion relies on the condition that both SI′ sites at one D_6R are occupied by Na^+ cations. With cations at SIII′ sites and H^+ forming bridging hydroxyl groups, the energy difference between fragments with Al−O−Si−O−Al linkages and those with Al−O−(Si−O)$_2$−Al linkages is less than 5 kJ mol^{-1}. The HOMO and LUMO electron density is redistributed upon Si,Al substitution and the localization of orbitals depends on the type and location of the extraframework charges. The oxygen atoms in proximity to the Brønsted acid sites emerge as Lewis basic sites.

Acknowledgment. The authors are grateful to Prof. G. St. Nikolov for many helpful discussions related to this study. Thanks are due to the Computer Center, Technical University, Vienna, where most of the Gaussian 98 calculations were performed.

References and Notes

(1) (a) Smith, J. V. *Chem. Rev.* **1988**, *88*, 149. (b) Meier, W. M.; Olson D. H. *Atlas of Zeolite Structure Types*; Butterworth: London, 1992.
(2) Newsam, J. M. In *Solid State Chemistry*: *Compounds*; Cheetham, A. K., Day, P., Eds.; Oxford University Press: New York, 1992; Vol. 2, p 234.
(3) Löwenstein, W. *Am. Mineral.* **1954**, *39*, 92.
(4) Dempsey, E. *J. Phys. Chem.* **1969**, *73*, 3660.
(5) Auf der Heyde, T.; Bürgi, H.-B.; Bürgi, H.; Tornroos, K. *Chimia* **1991**, *45*, 38.
(6) Bürgi, H.-B.; Bürgi, H.; Calzaferri, G.; Tornroos, K. *Inorg. Chem.* **1993**, *32*, 4914.
(7) Montero, M.; Voigt, A.; Teichert, M.; Uson, I.; Roesky, H. *Angew. Chem., Int. Ed. Engl.* **1995**, *34*, 2504.
(8) Calzaferri, G.; Hoffmann, R. *J. Chem. Soc., Dalton Trans.* **1991**, 917.
(9) (a) Earley, C. *Inorg. Chem.* **1992**, *31*, 1250. (b) Earley, C. *J. Phys. Chem.* **1994**, *98*, 8693.
(10) (a) Tossell, J. *Inorg. Chem.* **1998**, *37*, 2223. (b) Tossell, J. *J. Phys. Chem.* **1996**, *100*, 14828.
(11) Higgins, F. M.; Watson, G. W.; Parker, S. C. *J. Phys. Chem. B* **1997**, *101*, 9964.
(12) Uzunova, E. L.; Nikolov, G. S. *J. Phys. Chem. A* **2000**, *104*, 5302.
(13) Xiang, K.-H.; Pandey, R.; Pernisz, U.; Freeman, C. *J. Phys. Chem. B* **1998**, *102*, 8704.
(14) Engelhardt, G.; Michel, D. *High-Resolution Solid State NMR of Silicates and Zeolites*; Wiley: Chichester, U.K., 1987.
(15) Engelhardt, G.; Lohse, U.; Lipmaa, E.; Tarmak, M.; Mägi, M. *Z. Anorg. Allg. Chem.* **1981**, *482*, 49.
(16) Ramdas, S.; Thomas, J. M.; Klinowski, J.; Fyfe, C. A.; Hartman, J. S. *Nature* **1981**, *292*, 228.
(17) Peters, A. W. *J. Phys. Chem.* **1982**, *86*, 3489.
(18) Klinowski, J.; Ramdas, S.; Thomas, J. M.; Fyfe, C. A.; Hartman, J. S. *J. Chem. Soc., Faraday Trans. 2* **1982**, *78*, 1025.
(19) Melchior, M. T.; Vaughan, D. E. W.; Pictroski, C. F. *J. Phys. Chem.* **1995**, *99*, 6128.
(20) Vega, A. *ACS Symp. Ser.* **1983**, *218*, 217.
(21) Nagy, J. B.; Engelhardt, G.; Michel, D. *Adv. Colloid Interface Sci.* **1985**, *23*, 67.
(22) (a) Takaishi, T. *J. Phys. Chem.* **1995**, *99*, 10982. (b) Takaishi, T.; Kato, M.; Itabashi, K. *Zeolites* **1995**, *15*, 21.
(23) (a) Smith, J. V. *J. Chem. Soc.* **1964**, 3759. (b) Smith, L.; Eckert, H.; Cheetham, A. K. *Chem. Mater.* **2001**, *13*, 385. (c) Smith, L.; Eckert, H.; Cheetham, A. K. *J. Am. Chem. Soc.* **2000**, *122*, 1700.
(24) Jaramillo, E.; Auerbach, S. M. *J. Phys. Chem. B* **1999**, *103*, 9589.
(25) Buttefey, S.; Boutin, A.; Mellot-Draznieks, C.; Fuchs, A. H. *J. Phys. Chem. B* **2001**, *105*, 9569.
(26) Himei, H.; Yamadaya, M.; Oumi, Y.; Kubo, M.; Stirling, A.; Vetrivel, R.; Broclawik, E.; Miyamoto, A. *Microporous Mater.* **1996**, *7*, 235.
(27) Frisch, M. J.; Trucks, G. W.; Schlegel, H. B.; Scuseria, G. E.; Robb, M. A.; Cheeseman, J. R.; Zakrzewski, V. G.; Montgomery, J. A., Jr.; Stratmann, R. E.; Burant, J. C.; Dapprich, S.; Millam, J. M.; Daniels, A. D.; Kudin, K. N.; Strain, M. C.; Farkas, O.; Tomasi, J.; Barone, V.; Cossi, M.; Cammi, R.; Mennucci, B.; Pomelli, C.; Adamo, C.; Clifford, S.; Ochterski, J.; Petersson, G. A.; Ayala, P. Y.; Cui, Q.; Morokuma, K.; Malick, D. K.; Rabuck, A. D.; Raghavachari, K.; Foresman, J. B.; Cioslowski, J.; Ortiz, J. V.; Stefanov, B. B.; Liu, G.; Liashenko, A.; Piskorz, P.; Komaromi, I.; Gomperts, R.; Martin, R. L.; Fox, D. J.; Keith, T.; Al-Laham, M. A.; Peng, C. Y.; Nanayakkara, A.; Gonzalez, C.; Challacombe, M.; Gill, P. M. W.; Johnson, B. G.; Chen, W.; Wong, M. W.; Andres, J. L.; Head-Gordon, M.; Replogle, E. S.; Pople, J. A. *Gaussian 98*, revision A.7; Gaussian, Inc.: Pittsburgh, PA, 1998.
(28) Lee, C.; Yang, W.; Parr, R. G. *Phys. Rev.* **1988**, *B37*, 785−789.
(29) Miehlich, B.; Savin, A.; Stoll, H.; Preuss, H. *Chem. Phys. Lett.* **1989**, *157*, 200.
(30) Becke, A. D. *J. Chem. Phys.* **1993**, *98*, 5648.
(31) Mortier, W. J. *Compilation of Extraframework Sites in Zeolites*; Butterworth Science Ltd.: Guildford, U.K., 1982.
(32) Olson, D. H. *Zeolites* **1995**, *15*, 439.
(33) Vitale, G.; Mellot, C. F.; Bull, L. M.; Cheetham, A. K. *J. Phys. Chem. B* **1997**, *101*, 4559.
(34) Zhu, L.; Seff, K. *J. Phys. Chem. B* **1999**, *103*, 9512.
(35) (a) Zhu, L.; Seff, K. *J. Phys. Chem. B* **2000**, *104*, 8946. (b) Zhu, L.; Seff, K. *J. Phys. Chem. B* **2001**, *105*, 12221.
(36) Pierloot, K.; Delabie, A.; Ribbing, C.; Verberckmoes, A.; Schoonheydt, R. *J. Phys. Chem. B* **1998**, *102*, 10789.
(37) Schröder, K.-P.; Sauer, J. *J. Phys. Chem.* **1996**, *100*, 11043.
(38) Fogarasi, G.; Hacker, H.; Hoffmann, V.; Dobos, S. *Spectrochim. Acta, Part A* **1974**, *30A*, 629.
(39) Clegg, W.; Sheldrick, G. M.; Vater, N. *Acta Crystallogr. B* **1980**, *36*, 3162.
(40) Pluth, J.; Smith, J. *Mater. Res. Bull.* **1972**, *7*, 1311.
(41) Vitale, G.; Bull, L. M.; Morris, R.; Cheetham, A. K.; Toby, B.; Coe, C. *J. Phys. Chem.* **1995**, *99*, 16087.
(42) Sierka, M.; Sauer, J. *Faraday Discuss.* **1997**, *106*, 41.
(43) Hill, J.-R.; Freeman, C.; Delley, B. *J. Phys. Chem. A* **1999**, *103*, 3772.
(44) Beck, K.; Pfeifer, H.; Staudte, B. *Microporous Mater.* **1993**, *2*, 1.
(45) Czjzek, M.; Jobic, H.; Fitch, A. N.; Vogt, T. *J. Phys. Chem.* **1992**, *96*, 1535.
(46) Fenzke, D.; Hunger, M.; Pfeifer, H. *J. Magn. Reson.* **1991**, *95*, 477.
(47) (a) Eulemberger, G. R.; Shoemaker, D. P.; Keil, J. G. *J. Phys. Chem.* **1967**, *71*, 1812. (b) van Dun, J. J.; Dhaeze, K.; Mortier, W. J. *J. Phys. Chem.* **1988**, *92*, 6747. (c) Jirák, Z.; Vratislav, S.; Bosácek, V. *J. Phys. Chem. Solids* **1980**, *41*, 1089. (d) Marra, G. L.; Fitch, A. N.; Zeccina, A.; Ricciardi, G.; Salvalaggio, M.; Bordiga, S.; Lamberti, C. *J. Phys. Chem. B* **1997**, *101*, 10653. (e) Fitch, A. N.; Jobic, H.; Renouprez, A. *J. Phys. Chem.* **1986**, *90*, 1311.
(48) Shannon, R. *Acta Crystallogr. A* **1976**, *32*, 751.
(49) Deem, M. W.; Newsam, J. M.; Creighton, J. A. *J. Am. Chem. Soc.* **1992**, *114*, 7198.
(50) Peterson, B. K. *J. Phys. Chem. B* **1999**, *103*, 3145.